Size effects in surface-reconstructed ⟨100⟩ and ⟨110⟩ silicon nanowires

R. Rurali

Laboratoire Collisions, Agrégats, Réactivité, IRSAMC, Université Paul Sabatier,
118 Route de Narbonne, 31062 Toulouse Cedex, France
and Departament d'Enginyeria Electrònica, Universitat Autònoma de Barcelona, 08193 Bellaterra, Spain

A. Poissier and N. Lorente

Laboratoire Collisions, Agrégats, Réactivité, IRSAMC, Université Paul Sabatier, 118 Route de Narbonne,
31062 Toulouse Cedex, France

The geometrical and electronic structure properties of ⟨100⟩ and ⟨110⟩ silicon nanowires in the absence of surface passivation are studied by means of density-functional calculations. As we have shown in a recent publication [R. Rurali and N. Lorente, Phys. Rev. Lett. **94**, 026805 (2005)] the reconstruction of facets can give rise to surface metallic states. In this work, we analyze the dependence of geometric and electronic structure features on the size of the wire and on the growth direction.

I. INTRODUCTION

In recent years one-dimensional quantum systems have attracted great interest as building blocks for future molecular electronics devices. Besides proposed applications, there is also a fundamental interest in these systems, because as the size is reduced down to the nanoscale a description at the quantum level is necessary to account for most of the properties of the material.

Carbon nanotubes are certainly the most studied one-dimensional quantum systems. However, the dependence of their electronic properties on their diameter and on their chirality—and the difficulty of controlling such properties during growth—might make them an impractical choice for nanodevice engineering. Semiconductor nanowires seem to obviate such an inconvenience and they are becoming the focus of a growing research interest. Silicon nanowires (SiNWs) are an especially appealing choice, as they offer the best possible interface with conventional silicon-based microelectronics.

SiNWs have been successfully doped with both *n*- and *p*-type impurities[1–4] and nanoscale logic devices have been demonstrated.[5,6] A growing research interest has been devoted to the synthesis of SiNW-based heterostructures—oriented to optoelectronics applications[7] as well to device fabrication[8,9]—and to the use of SiNWs as chemical sensors.[10–13] At present, diameters around 100 nm thick can be almost routinely obtained and a few examples of SiNWs below 10 nm have been published,[14–17] 1.5 nm being the thinnest wire's diameter reported so far.[18]

Theoretically, at first the attention was directed to the structure of the thinnest possible SiNWs. Hollow structures[19] and systems ranging from atomic wires to silicon cluster aggregates have been proposed.[20] However, a wealth of experimental results[15,18,21] soon showed that realistic SiNWs present a well-defined diamondlike bulk core. Since then, significant efforts have been devoted to the modeling of hydrogen-passivated SiNWs,[22–27] i.e., wires where the lateral surface dangling bonds are terminated with hydrogens. These are extremely interesting systems for theoretical modeling for different reasons: (a) the absence of surface states allows an easier approach to the study of all the features related to quantum confinement,[22,24,25,27] e.g., the energy band gap is well-defined and depends only on the growth direction and on the wire diameter; and (b) it is a good approach to realistic experimental conditions where different kinds of polluting agents, e.g., hydrogen,[18] and oxygen,[28] are present and can react with the surface dangling bonds.

However, studying the surface physics of these low-dimensional systems without passivation is of great interest because of the subtle interplay between an unusually large surface-to-bulk ratio and the effect of quantum confinement. In a previous publication[29] we have shown that in the absence of passivation, the lateral surface of a ⟨100⟩ SiNW undergoes a strong reconstruction which can turn the wire metallic. The conductive surface states form at the {100} facets of the wire, at variance with the infinite Si(100) surface which is known to be semiconducting. Therefore the diameter of the SiNW must play a very crucial role in the determination of the surface electronic structure.

In this paper we analyze the diameter dependence of the surface reconstruction and of the associated electronic structure ⟨100⟩ SiNWs and we extend our study to wires grown along the ⟨110⟩ direction.

II. COMPUTATIONAL METHODS

We have performed density functional theory (DFT) calculations in the framework of the generalized gradient approximation (GGA).[30] We have used both numerical atomic orbital[31,32] and plane-wave methods[33] combined with norm-conserving pseudopotentials of the Troullier-Martins type[34] and with ultrasoft pseudopotentials, respectively. We have used a double-ζ polarized basis set[35–37] and a plane-wave cutoff of 20 Ry for the one-electron wave function of the valence electrons.

All the calculations use periodic boundary conditions, thus the supercell size may restrict the number of observed reconstructions. For this reason, to explore a larger set of the

phase space of the surface reconstruction we have also used a nonorthogonal tight-binding (TB) model[38,39] to treat system sizes that cannot efficiently be managed within DFT. Even in the cases when the TB surface electronic structure turned out to be only qualitatively accurate, the minimum energy geometries proved to be very close to those obtained by DFT. In all the calculations discussed, the atomic positions have been relaxed until the maximum force was lower than 0.04 eV/Å.

We have studied wires grown along the $\langle 100 \rangle$ direction of ~ 8, ~ 11, ~ 15, and ~ 27 Å and wires grown along the $\langle 110 \rangle$ direction of ~ 12, ~ 20, and ~ 26 Å, the ~ 8 and ~ 12 Å being the thinnest possible wires with a bulk core of each growth orientation. For each diameter considered we have carried out calculations with up to four unit cells of the un-reconstructed wire. The systems with the largest number of atoms (large diameter, many unit cells) have been only calculated with TB. The reciprocal space has been sampled with a converged number of k-points, ranging from 1 to 12, depending on the size of the unit cell in direct space.

After converging the atomic positions, we have recalculated the electronic structure with a three times thicker mesh of k-points and an *electronic temperature* approaching zero, in order to obtain a highly accurate band diagram, especially for what concerns the crossings of the Fermi level.

III. RESULTS AND DISCUSSION

A. $\langle 100 \rangle$ SiNWs

The first issue to deal with is the shape of the wire's cross section. Although we restrict to a specific growth direction, different sections are possible. We have discussed this topic elsewhere,[40] concluding that $\langle 100 \rangle$ SiNWs favor the formation of $\{100\}$ facets. On the other hand, we found that it is not clear if, at such small diameters, smoothing sharp angles increases or not the stability.[40] A discussion of the role of the edges can also be found in the work by Zhao and Yakobson[41] or by Ismail-Beigi and Arias.[42] Throughout this paper we will focus our attention on wires with smooth angles [see Figs. 1(a)–1(c)], even though most of the conclusions could be generalized to the case of wires with a square section (see Ref. 40 for a complete discussion).

The first $\langle 100 \rangle$ SiNW that we have analyzed has a diameter of ~ 8 Å. This size is well below the diameter of the thinnest SiNW grown so far (~ 15 Å, see Ref. 18), however, it can be a useful case study to elucidate the atomic scale mechanisms that are capable of inducing a metallic state at the wire's surface. We have found one only stable reconstruction which is illustrated in Fig. 2. It is characterized by one row of Si dimers along the z axis. The formation of Si dimers on the $\{100\}$ facets is a feature common to $\langle 100 \rangle$ SiNWs and is one of the characteristic reconstruction patterns of the infinite Si(100) surface.

The band structure diagram, displayed in Fig. 2, presents two states at the Fermi energy. It is well-known that DFT, though giving the correct dispersion of bands, underestimates band gaps. Therefore, especially in the case of marginal crossings of the Fermi level, it is difficult to guarantee the metallicity of the system. An accurate band-gap estimation can be obtained within the GW approximation (see, for
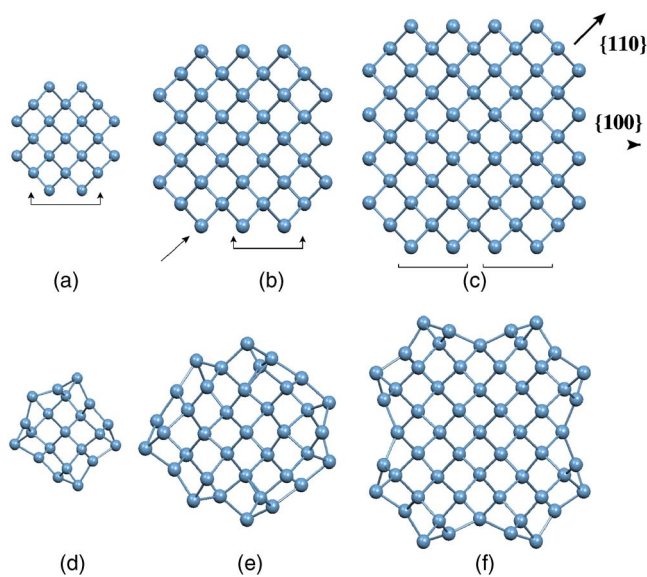

FIG. 1. (Color online) Section views of the unrelaxed [(a)–(c)] and relaxed [(d)–(f)] $\langle 100 \rangle$ SiNWs with a diameter of ~ 8, ~ 11, and ~ 15 Å. The facet geometry is determined by the number of rows of dimers (indicated by the brackets) that can form: (a,d) one-single row of dimers can form; (b,e) the formation of a second row of dimers is frustrated and the presence of an unpaired row of atoms results in an asymmetric relaxation of the facet; and (c,f) two rows of dimers form, yielding a *trough* in the middle of the $\{100\}$ facet.

instance, Ref. 27, where the effect of quantum confinement in semiconducting SiNWs is studied). For the purpose of the present work, the gap *renormalization* can be modeled with a scissor operator which rigidly shifts upward/downward the states above/below a certain energy. In the present case we cannot exclude that the proper scissor operator would open a small gap between the two states that in DFT electronic structure crosses the Fermi level, in such a way that the 8 Å SiNW would rather be a small-gap semiconductor.[29,40,43] Contrary to the band-widening effect of hydrogen-passivated wires, we notice that reconstructed wires present a reduction of the band gap as compared to the bulk value.

The most stable reconstruction[44] that we have found for the ~ 11 Å wire is shown in Figs. 1(e) and 3. It follows the same pattern of the previous wire, featuring one single row of dimers. The differences between these two cases are better understood looking at Figs. 1(a)–1(c), where the unrelaxed geometries are displayed. The thinnest wire can form only one row of dimers, involving all of the surface atoms of the $\{100\}$ facet [panel (a)]. The ~ 11 Å SiNW can also form only one row of dimers, but it leaves one unpaired row of Si atoms [panel (b)]. This has two notable effects: it results in a much more asymmetric in-plane relaxation [see Fig. 1(e)] and leaves a higher density of dangling bonds. The effects are clearly visible also in the side view of Figs. 2 and 3.

The asymmetry in the relaxation originates from the high reactivity of the surface atoms of the unpaired row. These atoms cannot form dimers, but their double dangling bonds would make the system unstable. The situation is depicted in Fig. 4: the gray atom (indicated with an arrow) eliminates one dangling bond by breaking a Si–Si subsurface bond (red
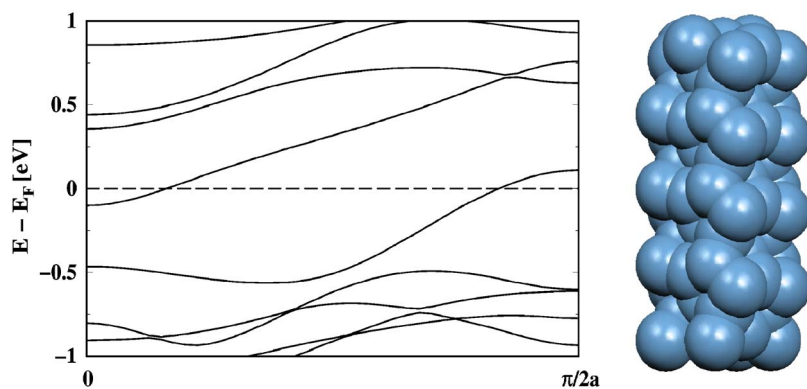
FIG. 2. (Color online) ⟨100⟩ SiNWs of ~8 Å diameter: side view of the reconstructed (pseudo) {100} facet.

atoms, also indicated with a circle in the picture) and *entering* it. The golden atoms (indicated with a cross in the picture) therein are strictly equivalent to the gray atom, but they can combine and form a dimer, according to the conventional mechanism of Si(100) surfaces.

The next ⟨100⟩ SiNW that we analyze has already been described in detail elsewhere.[29] In this case the diameter (~15 Å) starts to be sufficiently thick to permit one to distinguish clearly between a bulk region, consisting of atoms tetra-coordinated, and a surface region, consisting of atoms with lower coordination: the surface region is the one where the reconstruction occurs, while in the bulk region the atoms maintain the ideal position of the Si lattice.

In Ref. 29 we have shown that this wire sustains two different competing reconstructions, which only differ by 3 meV/atom. While one of them is strongly metallic, with four bands crossing the Fermi level, the other is at most semimetallic. In this case the assignment of a metallic character, at least to one of the two stable phases, is robust against failures of DFT, because two of the four metallic states are degenerate and thus cannot be shifted by a scissor operator without violating correct electron counting.[29]

This opens up a fundamental question: how can surface states of a {100} facet be metallic, while the analogous reconstruction of the Si(100) surface is semiconducting? In Fig. 5 we show a top view of the $c(4 \times 2)$ reconstruction of the Si(100) surface; it can be seen that by *cutting* a strip out of it, one recovers the metallic reconstruction of the {100} facet (the one referred to as *trough* or *1c* reconstruction in Ref. 29). However, the coordination of the boundary dimers changes because they now miss one of the *rest* atoms (some of them are indicated with an arrow in Fig. 5). This in turn

alters the packing density of the surface dimers, especially in the case of a nanometric size SiNW where *all* dimers are at the facet boundary. As a consequence of the altered packing density the dimers can couple and form surface states localized around the lower atoms of the dimers. In the other reconstruction that we have found,[29] some dimers are flipped, thus inhibiting the formation of such surface states. Hence, although the surface packing density is the same, in this case the wire is at most semimetallic or a small band-gap semiconductor. As the diameter of the wire is increased, a growing number of dimer rows will recover the coordination that they have on the Si(100) surface. Therefore when the fraction of dimers at the facet boundary becomes negligible a semiconducting behavior is expected.

The thicker ⟨100⟩ SiNW that we have studied has a diameter of approximately 27 Å. Up to this point we have distinguished between wires that have an even or an odd number of rows of dangling bonds in the {100} facets, because the different way of reducing the number of dangling bonds, i.e., forming dimers or through the mechanisms of Fig. 4, proved to be the most prominent factor ruling the reconstruction. In the wires discussed so far the dimers formed on the facet were characterized by an altered packing density (the mechanism is illustrated schematically in Fig. 5), which ultimately results in the metalization. In this wire three rows of dimers are formed on each {100} facet, so it is the first among the SiNWs that we have considered that features at least one row of dimers which has the same nearest-neighbor coordination than the infinite Si(100) surface. This situation is revealed by the band structure of Fig. 6 where, though still being metallic, the band gap starts opening, as can be seen by comparison with the 15 Å wire.[29] Another evidence of the size effect can be appreciated in the side panels of the same figure.
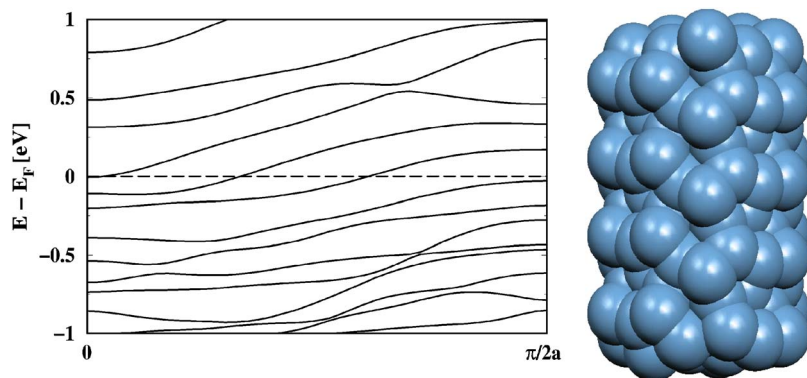

FIG. 3. (Color online) ⟨100⟩ SiNWs of ~11 Å diameter: side view of the reconstructed (pseudo) {100} facet.
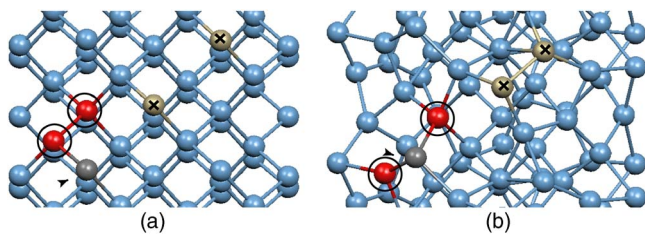
FIG. 4. (Color online) The mechanism that rules the facet relaxation when not all the dangling bonds can form dimers. The *gray* atom (indicated with an arrow) is unpaired and cannot form a dimer; to reduce the number of dangling bonds it breaks a bond of the underlying layer (*red* atoms, indicated with a circle) and enters it. The *golden* atoms (indicated with a cross) form a surface dimer according to the conventional mechanism of Si(100)-like surfaces.

There, we have plotted the wave function of the lower metallic state. It can be seen that the overlap between surface dangling bonds decreases for the larger diameter, indicating a higher localization of the surface state.

Summarizing, the metalization of $\langle 100 \rangle$ SiNWs is due to the partial distortion of the Si dimers on the {100} facets which alters the overall packing density with respect to the infinite Si(100) surface. When the fraction of dimers with the same coordination of the infinite surface increases, i.e., when the Si(100) packing density is recovered, the SiNW develops a semiconducting character.
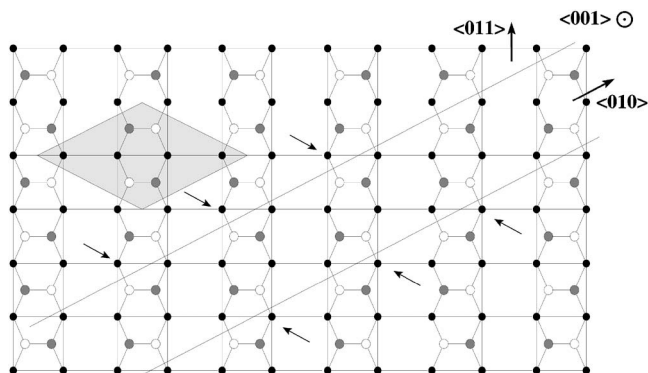

FIG. 5. Top view of the Si(100) $c(4 \times 2)$. White and gray balls represent the (asymmetric) top dimers, dark balls are the second layer atoms. A strip equivalent to the {100} facets of the ~15 Å $\langle 100 \rangle$ SiNW is drawn. Each of the atoms represented by white balls have only one second layer atom to rest onto (the missing ones are indicated with an arrow). This induces a tilt of the dimer axis when it relaxes, thus achieving a different packing density than the infinite Si(100) surface.

B. $\langle 110 \rangle$ SiNWs

In the case of $\langle 110 \rangle$ SiNWs the shape of the wire section is automatically defined by the hexagonal symmetry of the [110] plain of bulk Si. The hexagonal shape of the section of
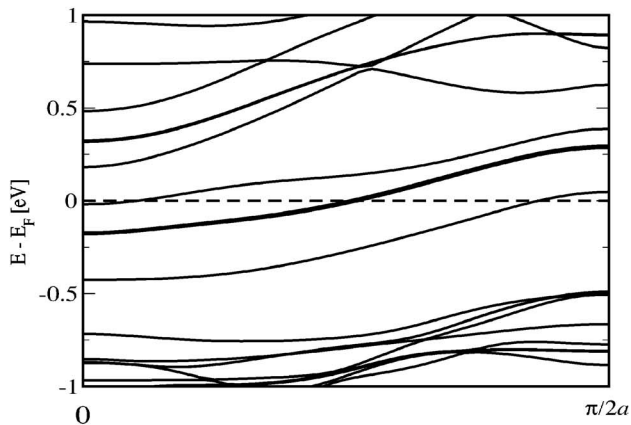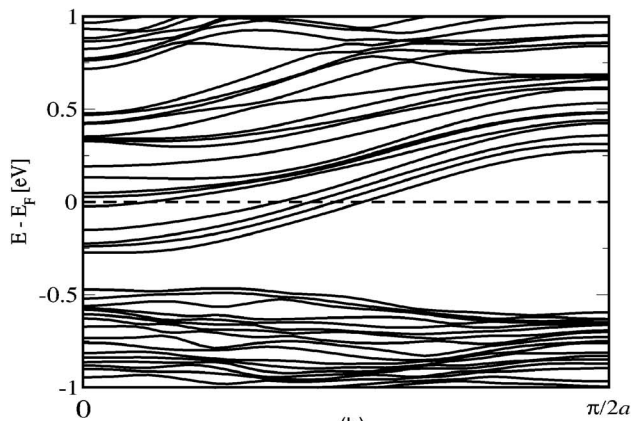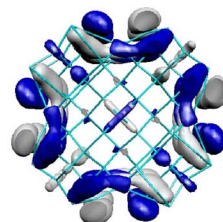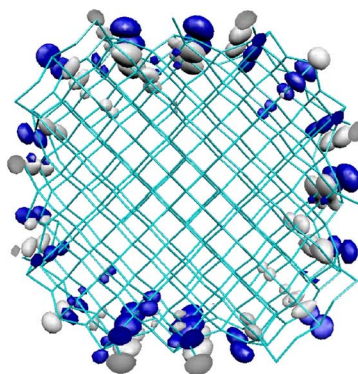

FIG. 6. (Color online) Band structure diagram of (a) the 15 Å SiNW of Ref. 29 and (b) the 27 Å SiNW. The comparison between the two panels shows the trend of the band-gap opening as the diameter is increased.
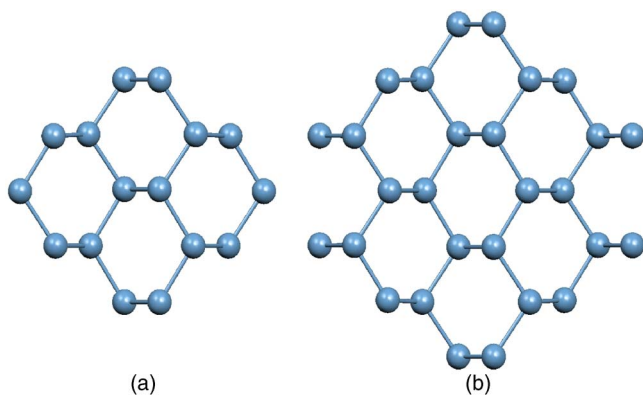
FIG. 7. (Color online) Possible geometries considered for ⟨110⟩ SiNWs. The section that features a central hexagon [shown in panel (b)] turned out to be the most stable.

⟨100⟩ SiNWs has been also confirmed unambiguously by scanning tunneling microscopy[18] and transmission electron microscopy[15] images. It should be stressed that in this case, contrary to ⟨100⟩ SiNWs, the angles between vicinal facets are intrinsically smooth. Hence the only issue concerning the cross section consists in choosing between two possible configurations, shown in Fig. 7: one with rings of hexagons organized around a single hexagonal channel and another without the central hexagon. We have carried out full relaxations of the atomic positions for the model structures of Fig. 7 and compared the cohesion energies [Eq. (3)]. The tests performed indicated that the arrangement in Fig. 7(b) is favored. Therefore this is the pattern that we have adopted to generate SiNWs with growing diameters (Fig. 8). Unfortunately, it is not possible to exclude that thicker wires would not favor different arrangements, but we needed a common model structure where to vary only the diameter. In these SiNWs the unrelaxed lateral surface is made up of {111} and
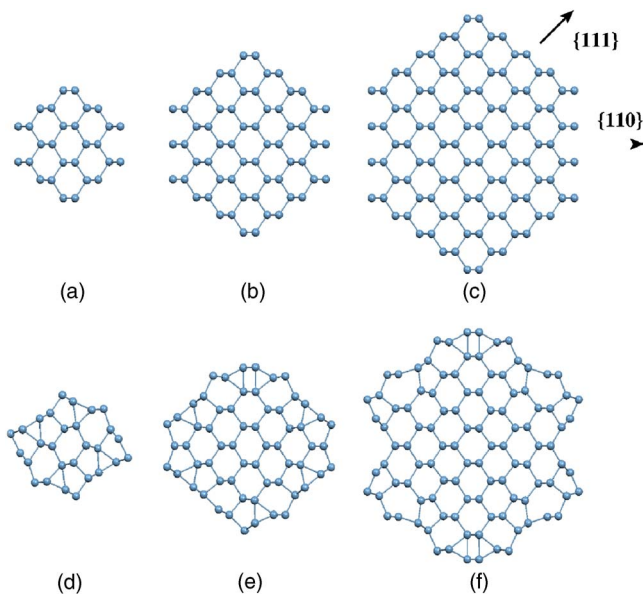

FIG. 8. (Color online) Section views of the unrelaxed [(a)–(c)] and relaxed [(d)–(f)] ⟨110⟩ SiNWs with a diameter of ∼12, ∼20, and ∼26 Å.
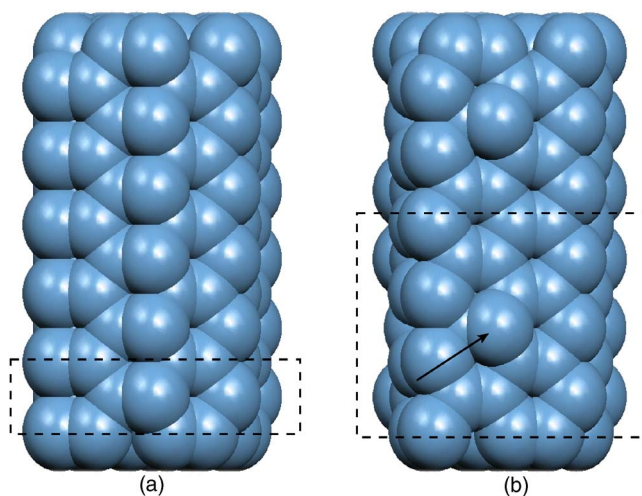

FIG. 9. (Color online) {111} facets of the two stable reconstructions that we have found for the 12 Å ⟨110⟩ SiNW. The different unit cells of the facet are indicated. The reconstructions have extension of (a) c and (b) $3c$, where c is the axial lattice parameter of the SiNW. In (a) the reconstruction features one row of aligned atoms, while in (b) only one atom of each three (indicated with an arrow) protrudes outward.

{110} facets. Therefore the competition mechanism that rules the reconstruction is expected to be markedly different to the case of ⟨100⟩ wires.

The thinnest ⟨110⟩ SiNW that we have studied turns out to have two competing reconstructions, which are shown in Fig. 9. After the relaxation it is hardly possible to still distinguish facets with a well-defined crystallographic orientation [see the top view of Fig. 8(d)]. The difference between the reconstructions found emerges at the {111}-like facets, where the periodicity of the protruding atoms change, as it can be observed in the space-fill representation of Fig. 9. The difference in energy is negligible, so that both reconstructions are expected to occur with the same probability. Most important, both phases are semiconducting with a small band gap, approximately one-third of its bulk value.

The ∼20 Å wire has similar features. It presents two reconstructions with a level of stability of the same order (the difference is around 3 meV/atom). In this case too, the rows of protruding atoms can arrange in different ways: one single row in the case of the reconstruction with the smallest motif; a second row which alternates protruding to nonprotruding atoms in the other reconstruction. Contrary to some of the cases described in Sec. III A, the differences in the reconstruction alter only marginally the band structure and a semiconducting character can be safely attributed to both phases.

Curiously, it turns out that the number of protruding atoms is always a constant. In the smallest reconstruction [Fig. 10(a)] none of the atoms protrude outward, while all of them do in the opposite facet (not shown here). The opposite point of view was chosen for the unit-cell reconstruction of Fig. 9(a), where all the atoms are protruding outward, while none of them does in the opposite facet. In the same way, the more varied motif of the extended reconstructions of Figs. 9(b) and 10(b) is echoed in the opposite facet, where a depressed atom corresponds to a protruding atom and vice versa.
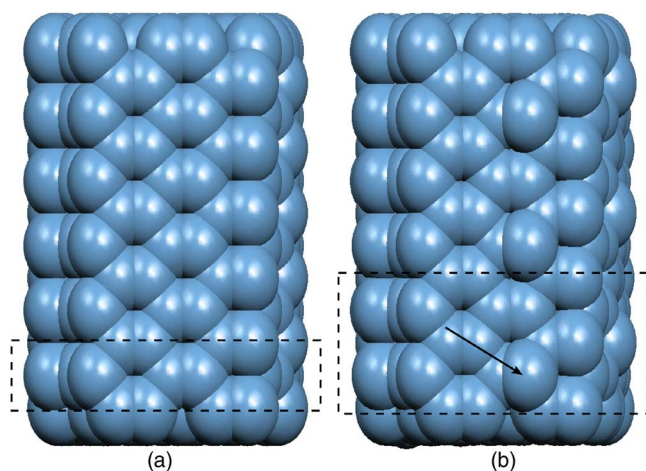
FIG. 10. (Color online) {111} facets of the two stable reconstructions of the 20 Å ⟨110⟩ SiNW. The different unit cells of the facet are indicated. The reconstructions have extension of (a) c and (b) $2c$, where c is the axial lattice parameter of the SiNW. In (a) the reconstruction features one row of aligned atoms, while in (b) only one atom of each two (indicated with an arrow) protrudes outward.

The largest ⟨100⟩ SiNW that we have analyzed has a diameter of ∼26 Å. A significant difference with the thinner wires described here is that the diameter has reached a critical size so that not only {111}, but also {110} facets are present. The latter reconstructs forming a long trough all along the wire axis, while the {111} have a pattern similar to those seen so far, with a row of protruding atoms.

A common feature that clearly emerges is that, although there is a dependence of the band-gap size on the wire diameter, in none of the ⟨100⟩ SiNWs that we have studied the facet reconstruction gives rise to surface metallic states like in the case of wires grown along the ⟨100⟩ direction. From the discussion of the results it appears that these wires are dominated by {111} facets and {110} facets form only on thick wires. We note, however, that recently it has been reported that ⟨100⟩ SiNWs can also sustain metallic reconstructions.[45] The different reconstructions are very sensitive to the actual number of surface atoms and Ref. [45] discusses results for 200-atom systems, while the wire of Fig. 8(f) has 208 atoms. The difference in eight surface atoms leads to important implications regarding surface reconstructions in agreement with the behavior of adatoms on the surface of semiconductors.

The found geometries—and their semiconducting character—agree with the π-bonded chain model typical of the 2×1 reconstruction of the Si(111) surface.[46–49] The unreconstructed surface (the facet in the case of the wire) features one dangling bond per atom and the system spontaneously reduces its symmetry to lower the energy of the half-occupied states. This is possible because the surface dangling bonds reside on nearest-neighbor atoms and the bond orbitals are close enough to interact significantly stabilizing the surface and introducing a band gap between occupied and unoccupied states.[47] Other reconstructions, notably the 7×7, are known to be metallic due to the presence of adatoms that have not been considered in the present study. Adatoms could lead to metallic—and possibly more stable—phases also in the case of nanowire facets and their influence on the electronic and geometrical structure of the reconstruction should be addressed. However, under a certain diameter the facets are not large enough to host such extended reconstructions, but the existence of adatom phases cannot be ruled out.

Further insight on the mechanisms that rule the surface physics of these wires can be obtained from the analysis of Fig. 11. In the left panel we have plotted the energy gained with the relaxation

$$\epsilon_{\text{rel}} = (E_{\text{tot}}^{\text{rec}} - E_{\text{tot}}^{\text{unrec}})/n, \tag{1}$$

where $E_{\text{tot}}^{\text{rec}}$ and $E_{\text{tot}}^{\text{unrec}}$ are the total energies of the reconstructed and unreconstructed geometry (shown in Figs. 1 and 8) of a wire of n atoms. The first thing to observe is that with the relaxation ⟨110⟩ wires lower their energy less than ⟨100⟩. This is in agreement with the reconstruction mechanisms previously discussed: ⟨110⟩ wires simply rearrange the topology of the surface dangling bonds to allow the formation of a π-bonded chain; ⟨100⟩ wires, on the other hand, go through a much stronger reconstruction of the facet, involving the formation of new bonds.

Both curves are fairly linear, with the remarkable exception of the 11 Å ⟨100⟩ SiNW. In the above discussion (see Sec. III A) we have suggested that facets of ⟨100⟩ SiNWs with an even number of dangling bond rows should be favored. In the opposite case (odd number of dangling bond rows, like the 11 Å wire), the system has to spend a larger amount of structural energy to readjust the facet geometry because it cannot form ordered rows of dimers. This intuitive idea is confirmed by Fig. 11(a) and becomes clearer by defining the surface energy as
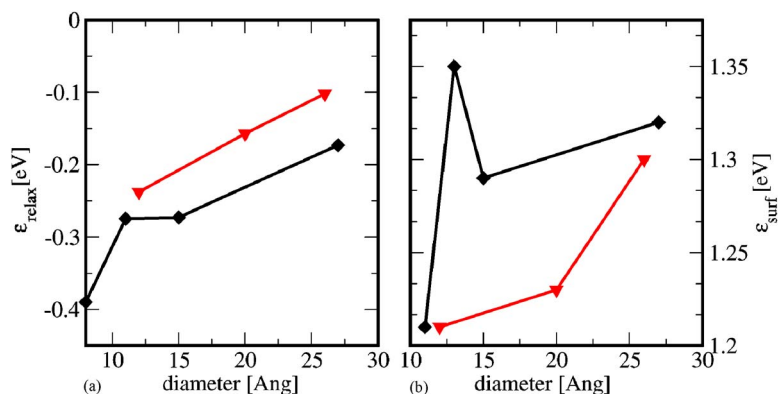

(a)

(b)

FIG. 11. (Color online) Energy gained with the relaxation, Eq. (1) (a) and surface energy, as defined in Eq. (2) (b). Black diamonds, ⟨100⟩ SiNWs; and red triangles, (110) SiNWs.

TABLE I. Cohesion energies of the SiNWs studied. For thin diameters ⟨110⟩ are favored, but as the size is increased the difference tends to disappear.

Orientation diameter (Å)	E_{coh} (eV)
⟨100⟩	
8	−3.75
11	−3.86
15	−3.99
27	−4.16
⟨110⟩	
12	−3.93
20	−4.08
26	−4.14

$$\epsilon_{surf} = (E_{tot} - n_{bulk}\epsilon_{bulk})/n_{surf}, \qquad (2)$$

where ϵ_{bulk} is the energy per atom of bulk Si and n_{bulk} and n_{surf} the number of bulk and surface atoms, respectively.[50] In this way, in the graph of Fig. 11(b) we isolated pure surface contributions and the *anomaly* of the 11 Å wire emerges in a more evident way.

As a concluding remark, we discuss the cohesion energies defined as[43]

$$\epsilon_{coh} = (E_{tot} - n\epsilon_{Si})/n, \qquad (3)$$

where E_{tot} is the total energy of the wire, n is the number of atoms, and ϵ_{Si} the energy of the isolated Si atom. The cohesion energy,[43] being directly derived from the total energy, allows one to compare the relative stabilities of the systems studied and which structures will be favored, in absence of other constraints, in the growth process (see Table I). The smoother angle between vicinal facets favors ⟨110⟩ growth orientation to the sharper angle of ⟨100⟩ SiNWs. When the diameter increases the difference tends to disappear: ⟨100⟩ wires reach a critical cross section that allows them to form smoother transition facets, while thick ⟨110⟩ wires start to develop their own {100} facets, which are expected to contribute with a surface energy very similar to the {100} facets of the ⟨100⟩ SiNWs.

Summarizing, the ⟨100⟩ SiNWs that we have analyzed turned out to be always semiconducting. The dangling bonds on the {111} facets cannot give rise to the formation of dimers because, due to the different symmetry of the cleavage, they are second neighbors. Incidentally, if they could form dimers this would result in a complete passivation of the wire because each atom on the facet surface has only one dangling bond per atom. However, the dangling bonds are close enough to interact and to form a π-bonded chain typical of Si(111) 2×1 surfaces.

IV. CONCLUSIONS

We have performed first-principles electronic structure calculations to study the surface reconstructions of ⟨100⟩ and ⟨110⟩ of different diameters.

SiNWs grown along the ⟨100⟩ axis are dominated by {100} facets that exhibit the typical reconstruction pattern of the Si(100) surface, consisting in the formation of rows of buckled dimers. In the case of the thinner wires, the altered packing density of the facet dimers gives rise to delocalized surface states that result in a metalization of the surface. Increasing the diameter, the coordination of the infinite Si(100) is recovered. The largest ⟨100⟩ SiNW studied, though still metallic, gives a clear indication of a band-gap opening.

The case of SiNWs grown along the ⟨110⟩ axis is different. Thanks to a different cross-section shape, the neighboring facets can match through a smooth angle and they are not significantly distorted with respect to their homologous infinite surfaces. Hence the {111} facets that dominate the reconstruction follow the π-bonded chain model of Si(111) surfaces, conferring to the wire a semiconducting character. The band gaps are found to be smaller than the bulk value as an effect of the formation of the π-surface states, while as it is well-known, H-passivated wire of similar sizes result in widened gaps as a consequence of quantum confinement. Analysis of the energetics of the wires indicates that at small diameters the growth of ⟨110⟩ SiNWs is favored over ⟨100⟩ SiNWs.

[1] Y. Cui, X. Duan, J. Hu, and C. M. Lieber, J. Phys. Chem. B **104**, 5213 (2000).

[2] Y. Cui, Z. Zhong, D. Wang, W. U. Wang, and C. M. Lieber, Nano Lett. **3**, 149 (2003).

[3] G. W. Zhou, H. Li, H. P. Sun, D. P. Yu, Y. Q. Wang, X. J. Huang, L. Q. Chen, and Z. Zhang, Appl. Phys. Lett. **75**, 2447 (1999).

[4] R. A. Beckman, E. Johnston-Halperin, N. A. Melosh, Y. Luo, J. E. Green, and J. R. Heath, J. Appl. Phys. **96**, 5921 (2004).

[5] Y. Cui and C. M. Lieber, Science **291**, 851 (2001).

[6] Y. Huang, X. F. Duan, Y. Cui, L. J. Lauhon, K. H. Kim, and C. M. Lieber, Science **294**, 1313 (2001).

[7] Y. Wu, R. Fan, and P. Yang, Nano Lett. **2**, 83 (2002).

[8] Y. Wu, J. Xiang, C. Yang, W. Lu, and C. M. Lieber, Nature (London) **430**, 61 (2004).

[9] L. J. Lauhon, M. S. Gudiksen, D. Wang, and C. M. Lieber, Nature (London) **420**, 57 (2002).

[10] Y. Cui, Q. Q. Wei, H. K. Park, and C. M. Lieber, Science **293**, 1289 (2001).

[11] F. Patolsky and C. M. Lieber, Mater. Today **8**, 20 (2005).

[12] X. T. Zhou, J. Q. Hu, C. P. Li, D. D. D. Ma, C. S. Lee, and S. T. Lee, Chem. Phys. Lett. **369**, 220 (2003).

[13] J. Hahm and C. M. Lieber, Nano Lett. **4**, 51 (2004).

[14] J. D. Holmes, K. P. Johnston, R. C. Doty, and B. A. Korgel, Science **287**, 1471 (2000).

[15] Y. Wu, Y. Cui, L. Huynh, C. J. Barrelet, D. C. Bell, and C. M. Lieber, Nano Lett. **4**, 433 (2004).

[16] N. R. B. Colemann, M. A. Morris, T. R. Spalding, and J. D. Holmes, J. Am. Chem. Soc. **123**, 187 (2001).

[17] N. R. B. Colemann, N. O'Sullivan, K. M. Ryan, T. A. Crowley, M. A. Morris, T. R. Spalding, D. C. Steytler, and J. D. Holmes, J. Am. Chem. Soc. **123**, 7010 (2001).

[18] D. D. D. Ma, C. S. Lee, F. C. K. Au, S. Y. Tong, and S. T. Lee, Science **299**, 1874 (2003).

[19] M. Menon and E. Richter, Phys. Rev. Lett. **83**, 792 (1999).

[20] B. X. Li, P. L. Cao, R. Q. Zhang, and S. T. Lee, Phys. Rev. B **65**, 125305 (2002).

[21] Y. F. Zhang, L. S. Liao, W. H. Chan, S. T. Lee, R. Sammynaiken, and T. K. Sham, Phys. Rev. B **61**, 8298 (2000).

[22] R. Q. Zhang, Y. Lifshitz, D. D. D. Ma, Y. L. Zhao, T. Frauenheim, S. T. Lee, and S. Y. Tong, J. Chem. Phys. **123**, 144703 (2005).

[23] T. L. Chan, C. V. Ciobanu, F. C. Chuang, N. Lu, C. Z. Wang, and K. M. Ho, Nano Lett. **6**, 277 (2006).

[24] B. Delley and E. F. Steigmeier, Appl. Phys. Lett. **67**, 2370 (1995).

[25] A. J. Read, R. J. Needs, K. J. Nash, L. T. Canham, P. D. J. Calcott, and A. Qteish, Phys. Rev. Lett. **69**, 1232 (1992).

[26] U. Landman, R. N. Barnett, A. G. Scherbakov, and P. Avouris, Phys. Rev. Lett. **85**, 1958 (2000).

[27] X. Zhao, C. M. Wei, L. Yang, and M. Y. Chou, Phys. Rev. Lett. **92**, 236805 (2004).

[28] N. Wang, Y. H. Tang, Y. F. Zhang, C. S. Lee, and S. T. Lee, Phys. Rev. B **58**, R16024 (1998).

[29] R. Rurali and N. Lorente, Phys. Rev. Lett. **94**, 026805 (2005).

[30] J. P. Perdew, K. Burke, and M. Ernzerhof, Phys. Rev. Lett. **77**, 3865 (1996).

[31] P. Ordejón, E. Artacho, and J. M. Soler, Phys. Rev. B **53**, R10441 (1996).

[32] J. M. Soler, E. Artacho, J. D. Gale, A. García, J. Junquera, P. Ordejón, and D. Sánchez-Portal, J. Phys.: Condens. Matter **14**, 2745 (2002); see also http://www.uam.es/siesta/.

[33] B. Hammer, L. B. Hansen, and J. K. Nørskov, Phys. Rev. B **59**, 7413 (1999); see also http://www.fysik.dtu.dk/campos/.

[34] N. Troullier and J. L. Martins, Phys. Rev. B **43**, 1993 (1991).

[35] E. Artacho, D. Sánchez-Portal, P. Ordejón, A. García, and J. M. Soler, Phys. Status Solidi B **215**, 809 (1999).

[36] J. Junquera, Ó. Paz, D. Sánchez-Portal, and E. Artacho, Phys. Rev. B **64**, 235111 (2001).

[37] E. Anglada, J. M. Soler, J. Junquera, and E. Artacho, Phys. Rev. B **66**, 205101 (2002).

[38] D. Porezag, T. Frauenheim, T. Köhler, G. Seifert, and R. Kaschner, Phys. Rev. B **51**, 12947 (1995).

[39] R. Rurali and E. Hernández, Comput. Mater. Sci. **28**, 85 (2003).

[40] R. Rurali and N. Lorente, Nanotechnology **16**, S250 (2005).

[41] Y. Zhao and B. I. Yakobson, Phys. Rev. Lett. **91**, 035501 (2003).

[42] S. Ismail-Beigi and T. Arias, Phys. Rev. B **57**, 11923 (1998).

[43] R. Rurali, Phys. Rev. B **71**, 205405 (2005).

[44] For this wire we have also found a different reconstruction. Though stable, it turned out to be more energetic than the one presented and hence it is not discussed here.

[45] M. V. Fernández-Serra, Ch. Adessi, and X. Blase, Phys. Rev. Lett. **96**, 166805 (2006).

[46] D. J. Chadi, Phys. Rev. Lett. **41**, 1062 (1978); Phys. Rev. B **26**, 4762 (1982).

[47] K. C. Pandey, Phys. Rev. Lett. **47**, 1913 (1981); **49**, 223 (1982).

[48] J. E. Northrup and M. L. Cohen, Phys. Rev. Lett. **49**, 1349 (1982).

[49] R. M. Feenstra, Phys. Rev. B **60**, 4478 (1999).

[50] There is an intrinsic ambiguity in the definition of Eq. (2), consisting in deciding which atoms are *surface* and which are *bulk* atoms. We have adopted a simple criterion according to which an atom is a surface atom whenever in the unrelaxed wire it had a coordination less than four. An alternative would be to consider surface atoms all those atoms which undergo a displacement during the relaxation larger than a certain threshold value. In such a case the 8 Å SiNW would be constituted exclusively by *surface atoms*, i.e., all the atoms move significantly in the relaxation.